International Journal of Heat and Mass Transfer 52 (2009) 1353–1364

Contents lists available at ScienceDirect

International Journal of Heat and Mass Transfer

journal homepage: www.elsevier.com/locate/ijhmt

Multi-Prandtl correlating equations for free convection heat transfer from a horizontal tube of elliptic cross-section

Massimo Corcione *, Emanuele Habib

Dipartimento di Fisica Tecnica, University of Rome "La Sapienza", via Eudossiana, 18, 00184 Rome, Italy

ARTICLE INFO

Article history:
Received 14 April 2008
Available online 14 October 2008

Keywords:
Free convection
Horizontal cylinder
Elliptic cross-section
Numerical analysis
Correlating equations

ABSTRACT

Steady laminar free convection from a horizontal elliptic cylinder set in unbounded space is studied numerically under the assumption of uniform surface temperature. A specifically developed computer-code based on the SIMPLE-C algorithm is used for the solution of the mass, momentum and energy transfer governing equations. Simulations are performed for ratios between the minor and major axes of the elliptic cross-section of the cylinder in the range between 0.05 and 0.98, inclination angles of the major axis of the elliptic cross-section with respect to gravity in the range between 0° and 90°, Rayleigh numbers based on the major axis of the elliptic cross-section in the range between 10 and 10^7, and Prandtl numbers in the range between 0.7 and 700. It is found that the heat transfer rate increases with increasing the Rayleigh and Prandtl numbers, while decreases with increasing the orientation angle of the cross-section of the cylinder, i.e., passing from the slender to the blunt configuration. In addition, a noteworthy fact is that in most cases the amount of heat exchanged at the cylinder surface has a peak at an optimum axis ratio which is practically independent of the Prandtl number, while may either increase or decrease with increasing the Rayleigh number depending on whether the orientation angle of the tube is above or below a critical value of approximately 67.5°. Dimensionless correlating equations are proposed both for the optimum axis ratio for maximum heat transfer and for the heat transfer rate from the cylinder surface to the undisturbed surrounding fluid reservoir.

1. Introduction

Free convection heat transfer from a horizontal cylinder to the surrounding fluid reservoir is of great practical importance in many engineering applications, as, e.g., high voltage power transmission lines, solar collectors, electronic devices, nuclear safety systems, and refrigeration condensers.

In the past decades, a considerable body of research has been conducted for circular cylinders, analytically, numerically, and experimentally, as clearly witnessed by the numerous data and heat transfer correlations available in the literature.

Among the pioneers, in 1912 Langmuir [1] published the results of extensive studies performed on free convection from thin wires in gases. He concluded that the heat transfer rate could be evaluated as the amount of heat conveyed by pure conduction through a film of stationary fluid surrounding the wire, which is the basic formulation of the so-called film theory. In 1954 McAdams [2] correlated many experimental data obtained by other workers for Rayleigh numbers in the range between 10^{-4} and 10^9. Correlating-equations based on existing experimental data across even wider ranges of the Rayleigh number were successively developed by Morgan [3], Churchill and Chu [4], and Kuehn and Goldstein [5]. Experiments were executed by Kutateladze [6], Pera and Gebhart [7], Hesse and Sparrow [8], Fand et al. [9], and Clemes et al. [10]. Analytical studies based on the boundary-layer approximation were conducted by Hermann [11], Chiang and Kaye [12], Saville and Churchill [13], Elliot [14], Merkin [15], and Muntasser and Mulligan [16]. Numerical solutions of the governing Navier–Stokes and energy equations were obtained by Kuehn and Goldstein [17], Farouk and Guceri [18], Badr [19], Wang et al. [20], and Saitoh et al. [21].

Investigations on free convection from horizontal cylinders of non-circular cross-section started in the early seventies, focusing a special attention upon the elliptic shape, mainly because it covers a wide extent of geometries which range between the two limiting cases of a flat plate and a circular cylinder.

The earliest work on this topic was performed by Lin and Chao [22], who employed a suitable coordinate transformation to solve the boundary-layer equations for two-dimensional and axisymmetric bodies of arbitrary contour in terms of series solutions. Local heat transfer results over horizontal elliptic cylinders were obtained for values of the ratio between the minor and major axes of the elliptic cross-section from 0.25 to 1, in both cases of slender and blunt orientations, i.e., with the major axis either vertical or horizontal, respectively, and for Prandtl numbers in the range between 0.72 and ∞. For circular and slender elliptic cylinders, it

* Corresponding author. Tel.: +39 06 44 58 54 43; fax: +39 06 48 80 120.
E-mail address: massimo.corcione@uniroma1.it (M. Corcione).

0017-9310/$ - see front matter © 2008 Elsevier Ltd. All rights reserved.
doi:10.1016/j.ijheatmasstransfer.2008.07.049

Nomenclature

a	major axis of the elliptic cross-section of the cylinder
b	minor axis of the elliptic cross-section of the cylinder
$\mathbf{g}$	gravity vector
g	gravitational acceleration
k	thermal conductivity of the fluid
L	dimensionless focal length of the elliptic cross-section of the cylinder
Nu	average Nusselt number
$Nu(\eta)$	local Nusselt number
P	perimeter of the elliptic cross-section of the cylinder
p	dimensionless pressure
Pr	Prandtl number = ν/α
Q	heat transfer rate
q	heat flux
Ra	Rayleigh number based on the major axis of the elliptic cross-section of the cylinder = $g\beta(t_w - t_\infty)a^3/\alpha\nu$
T	dimensionless temperature
t	temperature
U	dimensionless radial velocity component
$\mathbf{V}$	dimensionless velocity vector
V	dimensionless tangential velocity component
X	dimensionless Cartesian coordinate parallel to the major axis of the elliptic cross-section of the cylinder
x	Cartesian coordinate parallel to the major axis of the elliptic cross-section of the cylinder
Y	dimensionless Cartesian coordinate parallel to the minor axis of the elliptic cross-section of the cylinder
y	Cartesian coordinate parallel to the minor axis of the elliptic cross-section of the cylinder

Greek symbols

α	thermal diffusivity of the fluid
β	coefficient of volumetric thermal expansion of the fluid
η	dimensionless elliptic polar coordinate
φ	inclination angle of the major axis of the elliptic cross-section of the cylinder with respect to gravity
ν	kinematic viscosity of the fluid
ρ	density of the fluid
ξ	dimensionless elliptic radial coordinate
ξ_0	ξ-coordinate for the cylinder surface

Subscripts

c	referred to the circular cylinder
opt	optimum value
w	referred to the cylinder surface
0	referred to the vertical setting of the elliptic cross-section of the cylinder
90	referred to the horizontal setting of the elliptic cross-section of the cylinder
∞	referred to the undisturbed fluid

was found that the local Nusselt number has a maximum at the forward stagnation point, and decreases continuously as one moves downstream along the cylinder surface. In contrast, for blunt elliptic cylinders, the local Nusselt number increases as one moves away from the forward stagnation point, reaches a maximum at a location which corresponds to an eccentric angle of approximately 86°, and then decreases progressively up to the plume region. As regards the effect of the axis ratio, i.e., the ratio between the minor and major axes of the cylinder, on the overall heat transfer performance, the results reported in the paper show that, depending on whether the major axis of the cylinder is vertical or horizontal, the average Nusselt number increases or decreases with decreasing the axis ratio. In addition, of interest is the fact that, for slender orientations, the local value of the ratio $Nu/Ra^{0.25}$ is practically independent of the axis ratio for $x/a > 0.2$, where x is the distance from the lower stagnation point measured along the cylinder surface and a is the length of the major axis of the elliptic cross-section.

Raithby and Hollands [23], following the film theory of Langmuir, proposed an approximate procedure for the prediction of the amount of heat exchanged by free convection at the surface of slender elliptic cylinders over a wide range of the Rayleigh number, with a vertical plate and a circular cylinder as special cases. Their method, developed to overcome most of the limits of applicability typical of the thin-layer analysis, consisted in a modification of the solutions of the boundary-layer equations, introduced in order to account for both the effect of thick boundary layers at low Rayleigh numbers and the influence of turbulence at higher Rayleigh numbers. Its application was based on the calculation of the local thickness of the stationary fluid layer of variable thickness surrounding the body, and the subsequent solution for the conduction heat transfer across this so-called conduction layer. The results obtained for the elliptic cylinder were in a substantial good agreement with the Lin–Chao calculations. The Raithby–Hollands method was then simplified by Hassani [24], who replaced the conduction layer of variable thickness with a conduction layer of uniform thickness, and, at same time, extended its application to asymmetric horizontal cylinders of any convex cross-section. Indeed, for the case of elliptic cylinders with major axis neither vertical nor horizontal, the Hassani method is not an easy-to-apply method, since the calculation of the vertical height of the cylinder cross-section, required for the evaluation of the characteristic length in the Nusselt and Rayleigh numbers, is not immediate at all, which represents a limitation to its practical use.

The thin-layer approach was used also by Merkin [25], who wrote the boundary-layer equations in finite-difference form and solved them iteratively by the Newton–Raphson method. Local and average heat transfer results of the same type of those derived by previous workers were obtained for both slender and blunt orientations, under the assumption of either uniform surface temperature or uniform heat flux, for $Pr = 1$ and values of the axis ratio from 0.25 to 1. In accordance with the Lin–Chao results, it was found that for isothermal cylinders the slender orientation gives a higher average heat transfer to the fluid than the blunt orientation for the same value of the axis ratio and Rayleigh number. Recently, Cheng [26], following the work by Merkin, proposed a boundary-layer study in which he evaluated the effects of a temperature-dependent viscosity on both the heat transfer rate and the skin-friction.

The first well-documented experimental study on free convection from horizontal elliptic cylinders was conducted in 1984 by Huang and Mayinger [27], who performed interferometric measurements of the local and average heat transfer coefficients in air for axis ratios in the range between 0.364 and 0.667, Grashof numbers in the range between 4.5×10^4 and 3.77×10^5, and different orientations between the slender and blunt configurations. Among the several results obtained, it was observed that, as the inclination of the elliptic cross-section increases passing from the horizontal to the vertical setting of the major axis, the average Nusselt number of the cylinders with lower axis ratio increases much more than that for the cylinders with higher axis ratio. For the axisymmetric slender and blunt configurations, a heat correlation was also proposed.

Numerical solutions of the full conservation equations of mass, momentum and energy were derived by Badr and Shamsher [28] for a slender elliptic cylinder suspended in air, for different values of the Rayleigh number in the range between 10^{-2} and 10^3, and the axis ratio in the range between 0.1 and 0.964. It was found that for thin geometries, i.e., for axis ratios lower than 0.5, the minimum for the local value of the Nusselt number does not occur at the rear stagnation point, but at the sides of the elliptic cross-section; the lower is the Rayleigh number, the more the minimum for *Nu* is located toward the forward stagnation point (for an axis ratio of 0.5 and $Ra = 10^{-2}$, the minimum for *Nu* is reported to occur at approximately the endpoints of the horizontal minor axis of the cylinder cross-section).

Chen and Wang [29] performed a finite-difference numerical study for $Pr = 0.7$, Rayleigh numbers in the range between 10^2 and 10^6, axis ratios in the range between 0.25 and 1, and inclination angles in the range between 0° and 90°. Some experimental measurements based on holographic interferometry were carried out for two different elliptic tubes with axis ratios of 0.34 and 0.56, and for a circular cylinder, and used for validation. For the axisymmetric slender and blunt configurations, correlating equations for the average Nusselt number were developed.

Badr [30] conducted a numerical investigation of the transient natural convection from a horizontal elliptic tube in free air subjected to a sudden increase of its surface temperature, for axis ratios of 0.4, 0.6, 0.8, and 0.98, and orientation angles of 0°, 30°, 60°, and 90°, at the two Rayleigh numbers of 10^3 and 10^4. An interesting phenomenon reported is that at steady-state the maximum for the local Nusselt number occurs always at approximately the lower end of the major axis of the tube cross-section, regardless of the tube orientation. This extends what was already known for the slender configuration, in which the maximum for *Nu* occurs at the lowest point of the tube surface, i.e., the forward stagnation point, and for the blunt configuration, in which the maximum for *Nu* occurs at approximately the two endpoints of the horizontal major axis of the tube cross-section. In addition, it is worth mentioning that for the blunt configuration, at $Ra = 10^4$, a smooth maximum for the average Nusselt number was reported for the axis ratio of 0.6. Indeed, the author did not give importance to this, probably because of the lack of data available.

Works on the case of uniform heat flux were also conducted. Mahfouz and Kocabiyik [31] performed a numerical study of the transient buoyancy driven flow adjacent to a cylinder of elliptic cross-section with major axis horizontal, whose surface is subjected to a sudden uniform heat flux, for different values of the axis ratio in the range between 0.05 and 0.998, the modified Rayleigh number in the range between 10^3 and 10^7, and the Prandtl number in the range between 0.1 and 10. Elsayed et al. [32] executed experimental measurements in air on a single tube with a 0.555 axis ratio, for different values of the heat-flux-based Rayleigh number in the range between 1.1×10^7 and 8×10^7, and orientation angles in the range between 0° and 90°. In both papers, results consistent with data from prior researchers were reported.

The above review of the existing literature shows that numerous physical aspects of the problem have been studied and cleared, but only few workers have considered small axis ratios and inclinations of the elliptic cross-section different from the slender or the blunt orientations. In addition, most of the researchers have focused on relatively narrow ranges of the Rayleigh number, and on air as working fluid. Finally, only two authors proposed heat transfer correlations, which, in both cases, are related to only axisymmetric configurations.

In this background, the aim of the present paper is to carry out a numerical analysis of free convection from a horizontal tube of elliptic cross-section with isothermal surface, so as to derive heat transfer correlating equations spanning across sufficiently wide ranges of the independent variables to be of help in applications. The study is performed under the assumption of steady laminar flow, for axis ratios in the range between 0.05 and 0.98, orientation angles in the range between 0° (which corresponds to the slender configuration) and 90° (which corresponds to the blunt configuration), Rayleigh numbers in the range between 10 and 10^7, and Prandtl numbers in the range between 0.7 and 700.

2. Mathematical formulation

A horizontal cylinder of elliptic cross-section with major axis a and minor axis b is considered. The major axis is inclined an angle φ with respect to the gravity vector, as depicted in Fig. 1, in which a reference Cartesian system (x,y) is also represented. Free convection heat transfer occurs between the cylinder surface, kept at uniform temperature t_w, and the surrounding undisturbed fluid reservoir, assumed at uniform temperature t_∞.

The buoyancy-induced flow is considered to be steady and laminar. The cylinder is assumed to be much longer than the major axis, which implies that the end effects can be reasonably neglected and the temperature and velocity fields can be considered two-dimensional. The flow is assumed to be incompressible, with constant fluid properties and negligible viscous dissipation and pressure work. The buoyancy effects on momentum transfer are taken into account through the Boussinesq approximation.

Once the above assumptions are employed in the conservation equations of mass, momentum, and energy, the following set of dimensionless governing equations is obtained:

$$\nabla \cdot \mathbf{V} = 0 \tag{1}$$

$$(\mathbf{V} \cdot \nabla)\mathbf{V} = -\nabla p + \nabla^2 \mathbf{V} - \frac{Ra}{Pr} T \frac{\mathbf{g}}{g} \tag{2}$$

$$(\mathbf{V} \cdot \nabla)T = \frac{1}{Pr} \nabla^2 T \tag{3}$$

where $\mathbf{V}$ is the velocity vector having dimensionless velocity components U and V normalized with ν/a, T is the dimensionless temperature excess over the uniform temperature of the undisturbed fluid reservoir normalized with the temperature difference $(t_w - t_\infty)$, p is the dimensionless pressure normalized with $\rho_\infty \nu^2/a^2$, $Ra = g\beta(t_w - t_\infty)a^3/\alpha\nu$ is the Rayleigh number based on the major axis of the elliptic cross-section, $\mathbf{g}$ is the gravity vector, and $Pr = \nu/\alpha$ is the Prandtl number.

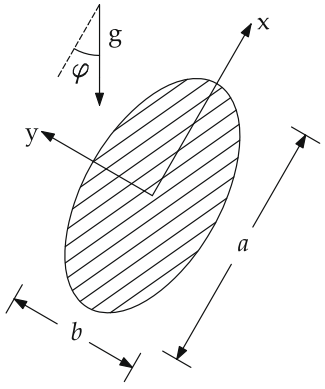

Fig. 1. Sketch of the tube geometry.

The related boundary conditions are $T = 1$ and $\mathbf{V} = 0$ on the cylinder surface, and $T = 0$ and $\mathbf{V} = 0$ at very large distance from the cylinder.

In order to work with coordinates appropriate to the tube geometry, a dimensionless elliptic coordinate system (ξ,η) is defined by the following transformations:

$$X = L\cosh\xi\cos\eta \tag{4}$$

$$Y = L\sinh\xi\sin\eta \tag{5}$$

where X and Y are the dimensionless Cartesian coordinates normalized with a, and L is the dimensionless focal length equal to $[1-(b/a)^2]^{0.5}/2$. In the (ξ,η) system, the ξ-constant lines are confocal ellipses with $\xi \geqslant \xi_0$, where ξ_0 is the ξ-coordinate for the cylinder surface, while the η-constant lines are confocal hyperbolae with $\eta \in [0,2\pi)$, as shown in Fig. 2. In this reference system, U is the radial velocity component, i.e., the component of $\mathbf{V}$ directed along the ξ-coordinate, and V is the tangential velocity component, i.e., the component of $\mathbf{V}$ directed along the η-coordinate. The value of ξ_0 is given by:

$$\xi_0 = \ln\frac{1+(b/a)}{\sqrt{1-(b/a)^2}} \tag{6}$$

The two-dimensional integration domain is assumed to extend up to a distance ξ_D from the cylinder surface sufficiently large to represent the so-called outer boundary. At such distance the fluid may reasonably be assumed to enter or leave the integration flow-domain in the direction normal to the confocal ellipse with $\xi = \xi_D$. The entering fluid is assumed at the undisturbed free field temperature. As regards the leaving fluid, whose temperature is not known a priori, a zero temperature gradient normal to the elliptic outer boundary is assumed, thus implying that the local heat transfer is dominated by convection rather than by conduction, provided that the outflow velocity is sufficiently high.

The following boundary conditions are then applied:

(a) at the cylinder surface, i.e., $\xi = \xi_0$ and $0 \leqslant \eta < 2\pi$:

$$U = 0, \quad V = 0, \quad T = 1 \tag{7}$$

(b) at the outer boundary of the computational domain, i.e., $\xi = \xi_D$ and $0 \leqslant \eta < 2\pi$:

$$\frac{\partial U}{\partial \xi} = 0, \quad V = 0, \quad T = 0 \text{ if } U \leqslant 0 \quad \text{or} \quad \frac{\partial T}{\partial \xi} = 0 \text{ if } U > 0 \tag{8}$$

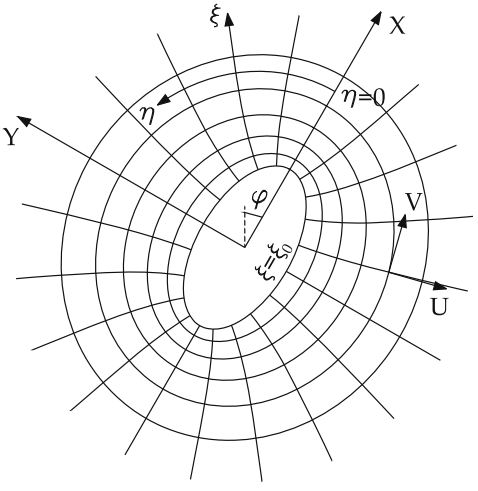

Fig. 2. Elliptic coordinate system.

3. Solution procedure

The set of governing equations (1)–(3) with the boundary conditions (7) and (8) is solved through a control-volume formulation of the finite-difference method. The pressure-velocity coupling is handled by the SIMPLE-C algorithm by Van Doormaal and Raithby [33], which is essentially a more implicit variant of the SIMPLE algorithm by Patankar and Spalding [34]. The advection fluxes are evaluated through the QUICK discretization scheme by Leonard [35]. Details on the SIMPLE procedure are widely available and well referenced in the literature (see, e.g., Patankar [36,37]).

A fine uniform mesh-spacing is used for the discretization in the η-direction, i.e., along the cylinder surface. In contrast, a variable spacing is used for the ξ-direction, providing for a concentration of grid lines near the cylinder surface and a relatively coarser resolution toward the outer boundary of the integration domain. Starting from assigned first-approximation fields of the dependent variables, the discretized governing equations are solved iteratively through a line-by-line application of the Thomas algorithm, enforcing under-relaxation to ensure convergence. The solution is considered to be fully converged when the maximum absolute values of both the mass source and the percentage changes of the dependent variables at any grid-node from iteration to iteration are smaller than the prescribed values, i.e., 10^{-5} and 10^{-6}, respectively.

After convergence is attained, the local and average Nusselt numbers $Nu(\eta)$ and Nu are calculated:

$$Nu(\eta) = \frac{qa}{k(t_w - t_\infty)} = -\left.\frac{\partial T}{\partial \xi}\right|_{\xi=\xi_0} \tag{9}$$

$$Nu = \frac{Qa}{kP(t_w - t_\infty)} = -\frac{1}{2\pi}\int_0^{2\pi}\left.\frac{\partial T}{\partial \xi}\right|_{\xi=\xi_0} d\eta \tag{10}$$

where q is the heat flux, Q is the heat transfer rate, P is the perimeter of the elliptic cross-section (which may be calculated through the Ramanujan's approximation [38]), and the temperature gradients at the cylinder surface are evaluated through a second-order profile among each wall-node and the next two corresponding fluid-nodes.

Tests on the dependence of the results obtained on the mesh-spacing, and on the extent of the integration domain, have been performed for several combinations of values of b/a, φ, Ra, and Pr. The optimal grid-size values, as well as the optimal position of the elliptic outer boundary used for computations, are such that further grid refinements or boundary displacements do not yield any noticeable modification neither in the heat transfer rates nor in the flow field, that is, the percentage changes of $Nu(\eta)$ and Nu, and the percentage changes of the maximum value of the tangential velocity component at $\eta = (90° + \varphi)$ and $(270° + \varphi)$, are smaller than the prescribed accuracy values, i.e., 0.5% and 1%, respectively. Typical features of the integration flow-domain may be summarized as follows: (a) the number of nodal points $(\xi \times \eta)$ lies in the range between 54×86 and 162×258, and (b) the major axis of the elliptic outer boundary of the computational domain varies between 4 and 20 times the major axis of the elliptic cross-section of the cylinder, depending on the Rayleigh and Prandtl numbers, the axis ratio, and the tilting angle. As far as the validation of the numerical code and the discretization grid system is concerned, the local Nusselt numbers $Nu(\eta)$ obtained from simulations performed for $Pr = 0.7$ are compared with: (a) the experimental data of Huang and Mayinger [27] for $Ra = 2 \times 10^5$, $b/a = 0.667$, and $\varphi = 0°$ and 90°, as reported in Figs. 3 and 4; (b) the numerical results of Badr and Shamsher [28] for $Ra = 10$, $b/a = 0.5$, and $\varphi = 0°$, as reported in Fig. 5; and (c) the numerical results of Badr [30] for $Ra = 10^3$, $b/a = 0.6$, and $\varphi = 30°$ and 60°, as reported in Figs. 6

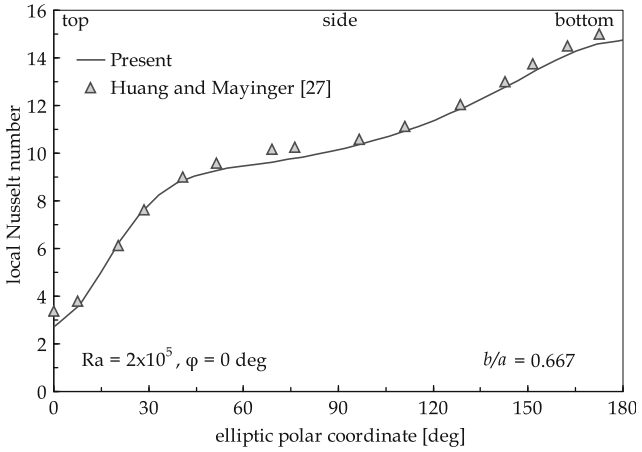

Fig. 3. Comparison between the present local results for $Pr = 0.7$, $Ra = 2 \times 10^5$, $b/a = 0.667$, and $\varphi = 0°$, and the experimental data by Huang and Mayinger [27].

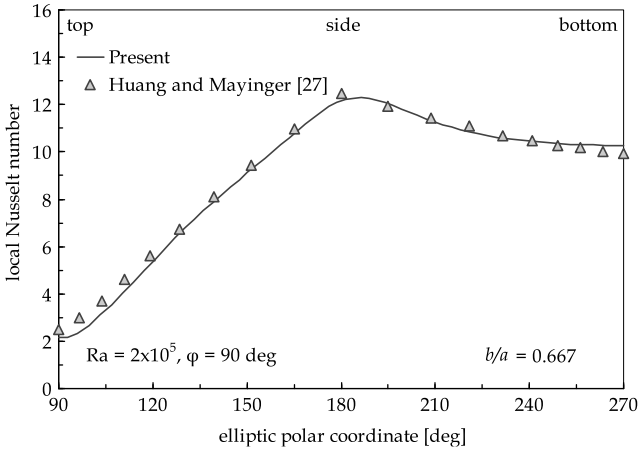

Fig. 4. Comparison between the present local results for $Pr = 0.7$, $Ra = 2 \times 10^5$, $b/a = 0.667$, and $\varphi = 90°$, and the experimental data by Huang and Mayinger [27].

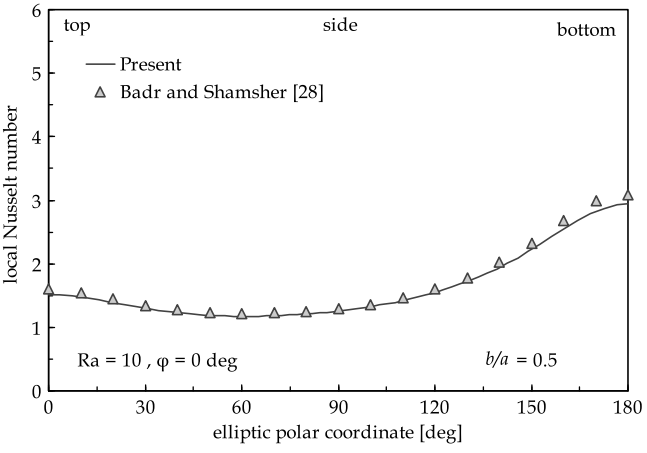

Fig. 5. Comparison between the present local results for $Pr = 0.7$, $Ra = 10$, $b/a = 0.5$, and $\varphi = 0°$, and the numerical data by Badr and Shamsher [28].

and 7. The results obtained for the average Nusselt number Nu are then compared with: (a) the numerical results of Badr [30] for $Pr = 0.7$, $b/a = 0.4$–0.98, $\varphi = 0°$ and 90°, and $Ra = 10^3$ and 10^4, as reported in Table 1; (b) the numerical results of Badr [30] for $Pr = 0.7$, $b/a = 0.6$, $\varphi = 0$–$90°$, and $Ra = 10^3$ and 10^4, as reported in Table 2;

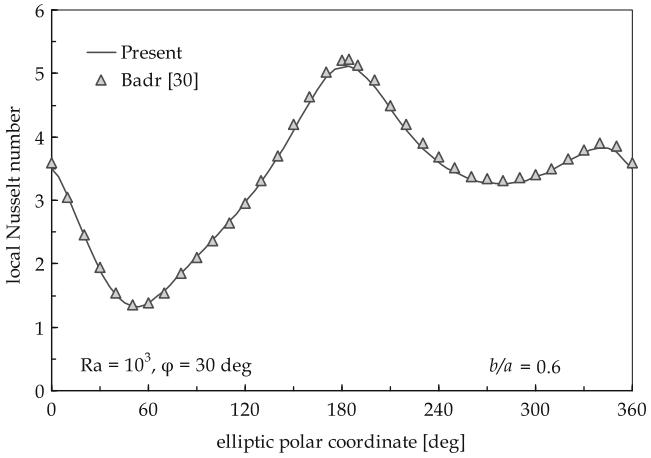

Fig. 6. Comparison between the present local results for $Pr = 0.7$, $Ra = 10^3$, $b/a = 0.6$, and $\varphi = 30°$, and the numerical data by Badr [30].

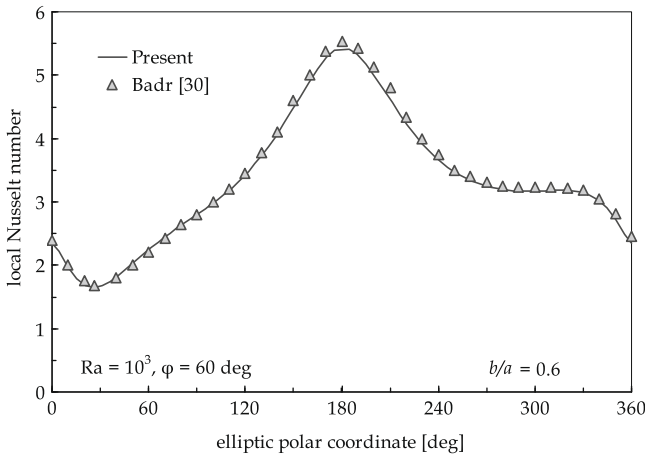

Fig. 7. Comparison between the present local results for $Pr = 0.7$, $Ra = 10^3$, $b/a = 0.6$, and $\varphi = 60°$, and the numerical data by Badr [30].

and (c) the analytical results of Raithby and Hollands [23] for $\varphi = 0°$, $b/a = 0.2$–0.98, Pr = 0.7–70, and $Ra = 10^4$ to 10^6, as reported in Table 3. An overall good degree of agreement between the present results and the literature data may be observed for both the local and the average Nusselt numbers, with percentage differences which in most cases do not exceed 1%. An exception is represented by the over-predictions of the Raithby–Hollands equation, whose average percentage order is 2.5%, with a few peaks of the order of 5–7%. However, these over-predictions were expected. In fact, the Raithby–Hollands correlation is based on boundary-layer solutions, and thus, even if these solutions were suitably improved by including the influence of the surface curvature, in some situations this correlation cannot take into full account the insulating effect of the flow separation from the cylinder surface.

4. Results and discussion

Numerical simulations are performed for different values of (a) the axis ratio b/a in the range between 0.05 and 0.98, (b) the orientation angle of the elliptic cross-section, φ, in the range between 0° (which corresponds to the slender configuration) and 90° (which corresponds to the blunt configuration), (c) the Rayleigh number based on the major axis, Ra, in the range between 10 and 10^7, and (d) the Prandtl number, Pr, in the range between 0.7 and 700.

Table 1
Comparison of the present solutions for the average Nusselt number with the numerical results of Badr [30] for slender and blunt elliptic cross-sections

$Pr = 0.7$		Nu			
Ra	b/a	$\varphi = 0°$		$\varphi = 90°$	
		Badr [30]	Present work	Badr [30]	Present work
10^3	0.4	3.59	3.54	3.20	3.15
	0.6	3.44	3.37	3.16	3.14
	0.8	3.23	3.19	3.11	3.09
	0.98	3.09	3.03	–	
10^4	0.4	5.91	5.69	4.90	4.89
	0.6	5.63	5.40	4.96	4.94
	0.8	5.36	5.11	4.93	4.90
	0.98	5.05	4.85	–	

Table 2
Comparison of the present solutions for the average Nusselt number with the numerical results of Badr [30] for inclined elliptic cross-sections

$Pr = 0.7$, $b/a = 0.6$		Nu	
Ra	φ (°)	Badr [30]	Present work
10^3	0	3.44	3.37
	30	3.35	3.33
	60	3.23	3.22
	90	3.16	3.14
10^4	0	5.63	5.40
	30	5.34	5.32
	60	5.11	5.09
	90	4.96	4.94

As said in Section 1, one of the main objectives of the present study is to develop dimensionless correlations useful in applications to heat transfer designers and constructors. To this end, what counts is not only to generate a numerous set of data across sufficiently wide ranges of the independent variables, but also to identify an adequate expression for such correlations, which must be suitable to take into proper account the varying dependence of the Nusselt number on any independent variable. In this perspective, the data analysis must point out both the general physical aspects of the transport phenomena investigated and all the features pertaining to the mathematical aspects of the results, that can give a further help to define a functional structure able to fit the heat transfer data as best as possible.

The present discussion of the results is then arranged in three distinct sections: the data obtained for $Pr = 0.7$, which corresponds to air, are reported and discussed first, in order to stress the effects of the orientation angle, axis ratio and Rayleigh number on the overall thermal performance of the elliptic cylinder; subsequently, emphasis is given to the effects of the Prandtl number; finally, a set of dimensionless heat transfer correlating equations is proposed.

4.1. Heat transfer in air ($Pr = 0.7$)

The effects of both the axis ratio b/a and the orientation angle φ on the average heat transfer rate from an elliptic cylinder suspended in free air are pointed out in Figs. 8–11, where some representative results are reported for $Ra = 10$, 10^3, 10^5, and 10^7, respectively. The ordinate of each diagram is the ratio Nu/Nu_c between the average Nusselt numbers for the elliptic cylinder and for the circular cylinder at same Rayleigh number, so as to highlight in what measure the shape and orientation of the cross-section of the cylinder either enhance or degrade its heat transfer performance relative to that of a circular tube – the Nusselt number of the circular cylinder for $10^1 \leqslant Ra \leqslant 10^7$ can be evaluated through the binomial correlation $Nu_c = 0.701 + 0.411Ra^{0.25}$, see Ref. [39].

It may be seen that for orientation angles below 60°, an enhancement of the order of 10–25% is the rule at any Rayleigh number investigated. In contrast, for larger inclinations the heat transfer performance may decrease, with a degree of degradation which increases with increasing both Ra and b/a.

In addition, it is worth pointing out that the amount of heat exchanged at the cylinder surface decreases as the orientation angle increases, which is due to the widening of the regions of the front and rear stagnation points. In particular, such degradation of the Nusselt number occurs at a rate which increases as the Rayleigh number increases and the axis ratio decreases. This may be explained by considering that the enlargements of the stagnation regions cited above become proportionally more significant with increasing Ra and decreasing b/a, as clearly reflected by the isotherm patterns plotted in Fig. 12, for $b/a = 0.5$, $\varphi = 0°$, 45°, and 90°, and $Ra = 10^2$, 10^4, and 10^6, and in Fig. 13, for $Ra = 10^4$, $\varphi = 0°$, 45°, and 90°, and $b/a = 0.2$, 0.5, and 0.8. An overview of the effects of both Ra and b/a on the rate of the decrease of the heat transfer performance, which occurs as the orientation angle φ passes from 0° to 90°, is presented in Fig. 14, where the distributions of the ratio Nu_{90}/Nu_0 between the average Nusselt numbers for the horizontal setting ($\varphi = 90°$) and for the vertical setting ($\varphi = 0°$) of the elliptic cross-section at same Rayleigh number and axis ratio, are plotted vs. Ra for different values of b/a in the range between 0.05 and 0.98.

Table 3
Comparison of the present solutions for the average Nusselt number with the data derived from the Raithby–Hollands correlating equation [23] for slender elliptic cross-sections

$\varphi = 0°$		Nu					
Ra	b/a	$Pr = 0.7$		$Pr = 7$		$Pr = 70$	
		R–H equation [23]	Present work	R–H equation [23]	Present work	R–H equation [23]	Present work
10^4	0.2	6.27	5.89	7.24	6.87	7.63	7.52
	0.4	5.95	5.69	6.87	6.63	7.24	7.22
	0.6	5.59	5.40	6.45	6.30	6.80	6.83
	0.8	5.25	5.11	6.07	5.95	6.39	6.44
	0.98	4.96	4.85	5.73	5.67	6.03	6.11
10^5	0.2	10.19	9.85	11.89	11.52	12.59	12.43
	0.4	9.70	9.45	11.31	11.06	11.96	11.93
	0.6	9.18	8.95	10.69	10.50	11.30	11.30
	0.8	8.71	8.44	10.14	9.92	10.69	10.66
	0.98	8.31	8.02	9.66	9.45	10.17	10.15
10^6	0.2	17.16	16.83	20.17	19.77	21.39	21.18
	0.4	16.47	16.10	19.31	18.94	20.43	20.30
	0.6	15.77	15.20	18.43	17.93	19.45	19.23
	0.8	15.18	14.34	17.68	16.94	18.60	18.18
	0.98	14.68	13.63	17.04	16.13	17.87	17.29

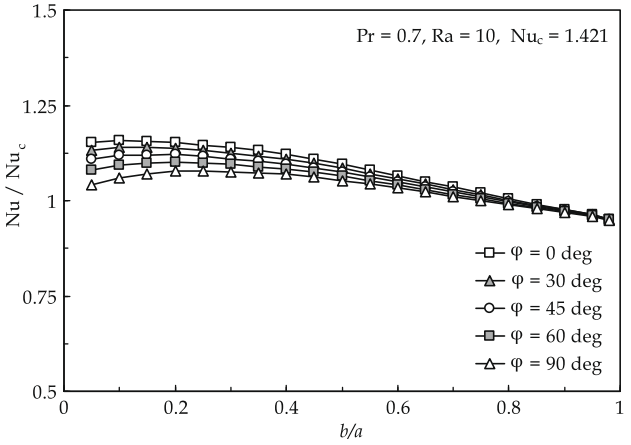

Fig. 8. Distributions of the ratio Nu/Nu_c vs. b/a for $Pr = 0.7$, $Ra = 10$ and different values of φ.

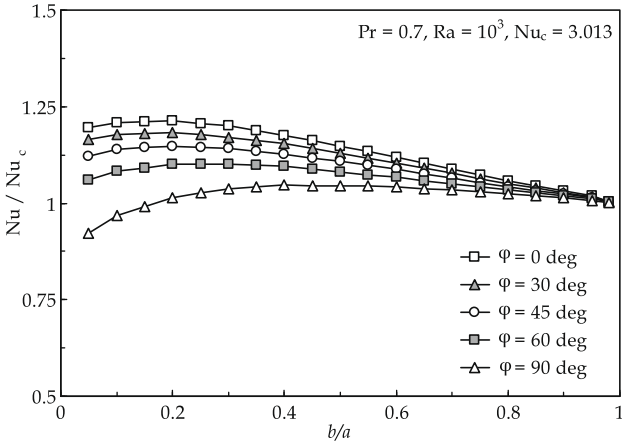

Fig. 9. Distributions of the ratio Nu/Nu_c vs. b/a for $Pr = 0.7$, $Ra = 10^3$ and different values of φ.

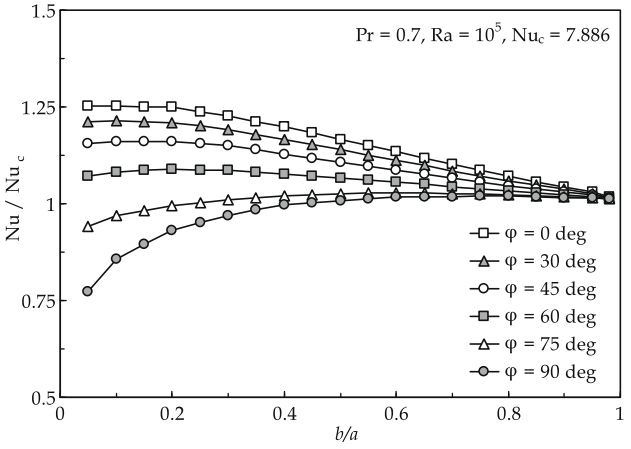

Fig. 10. Distributions of the ratio Nu/Nu_c vs. b/a for $Pr = 0.7$, $Ra = 10^5$ and different values of φ.

A further noteworthy fact is that in most cases the average Nusselt number has a peak at an optimum axis ratio $(b/a)_{opt}$, whose distributions vs. the orientation angle φ for different Rayleigh numbers are reported in Fig. 15. It may be observed that such optimum axis ratio may either increase or decrease with increasing the

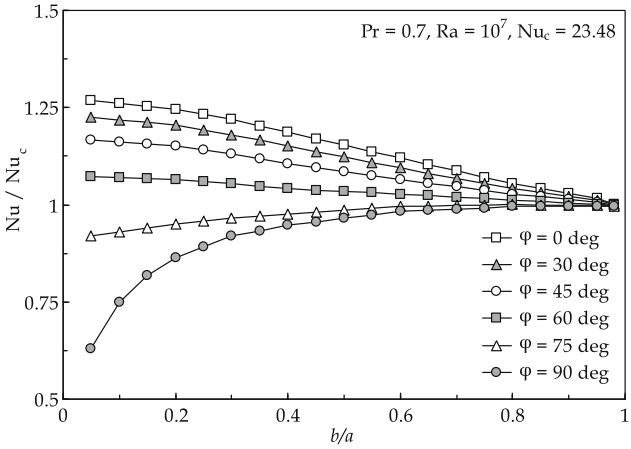

Fig. 11. Distributions of the ratio Nu/Nu_c vs. b/a for $Pr = 0.7$, $Ra = 10^7$ and different values of φ.

Rayleigh number, depending on whether the orientation angle is larger or smaller than a "critical" value $\varphi^* \cong 67.5°$ at which $(b/a)_{opt}$ is approximately 0.33, independently of the Rayleigh number.

Finally, as expected, the Nusselt number increases with increasing the Rayleigh number, which is due to the buoyancy increase. In particular, the increase of Nu with Ra occurs with a slope which decreases or increases with increasing the axis ratio, depending on whether the tube configuration is either slender or blunt.

4.2. Heat transfer in liquids ($0.7 < Pr \leqslant 700$)

The effects of the Prandtl number on the heat transfer rate at the cylinder surface are pointed out in Fig. 16, where the distributions of Nu vs. Ra for $b/a = 0.5$ and $\varphi = 45°$ are reported for different Prandtl numbers, and in Figs. 17 and 18, where the distributions of Nu vs. b/a for $Ra = 10^4$, and different Prandtl numbers, are reported for $\varphi = 15°$ and $\varphi = 75°$, respectively (in all the figures the Nu-distributions for $Pr = 0.7$ are also represented for comparison).

It may be noticed that the average Nusselt number increases with increasing the Prandtl number, with a decreasing gradient, which is typical for intermediate Prandtl numbers, as clearly reflected by the isotherm patterns depicted in Fig. 19 for $Ra = 10^4$, $b/a = 0.5$, $\varphi = 45°$, and $Pr = 0.7$, 7, 70, and 700. It is apparent that, as the Prandtl number is increased, the increased viscosity effect brings to an increase of the temperature gradients at the cylinder surface, and to a contraction of the rear stagnation region where the buoyant plume is rooted.

In addition, it may be seen that the distributions of the average Nusselt number for liquids maintain the same trends of those already derived for air, that is, once Ra and φ are assigned, the Nu-distributions corresponding to different Prandtl numbers are parallel to one another. This means that at any Rayleigh number and inclination of the elliptic cross-section with respect to gravity, the optimum axis ratio remains substantially unchanged with Pr, i.e., remains the same as that derived for $Pr = 0.7$. In particular, the critical orientation angle φ^* and $(b/a)_{opt}$ at such critical angle φ^* maintain the same values as those previously obtained for air, i.e., nearly 67.5° and 0.33, respectively.

4.3. Correlations for the optimum axis ratio

According to what has been said above, the optimum axis ratio $(b/a)_{opt}$ is a function of only Ra and φ, being practically independent of Pr. The best-fit of all the values obtained for $(b/a)_{opt}$ is given by the following semi-empirical correlations, as shown in Fig. 20:

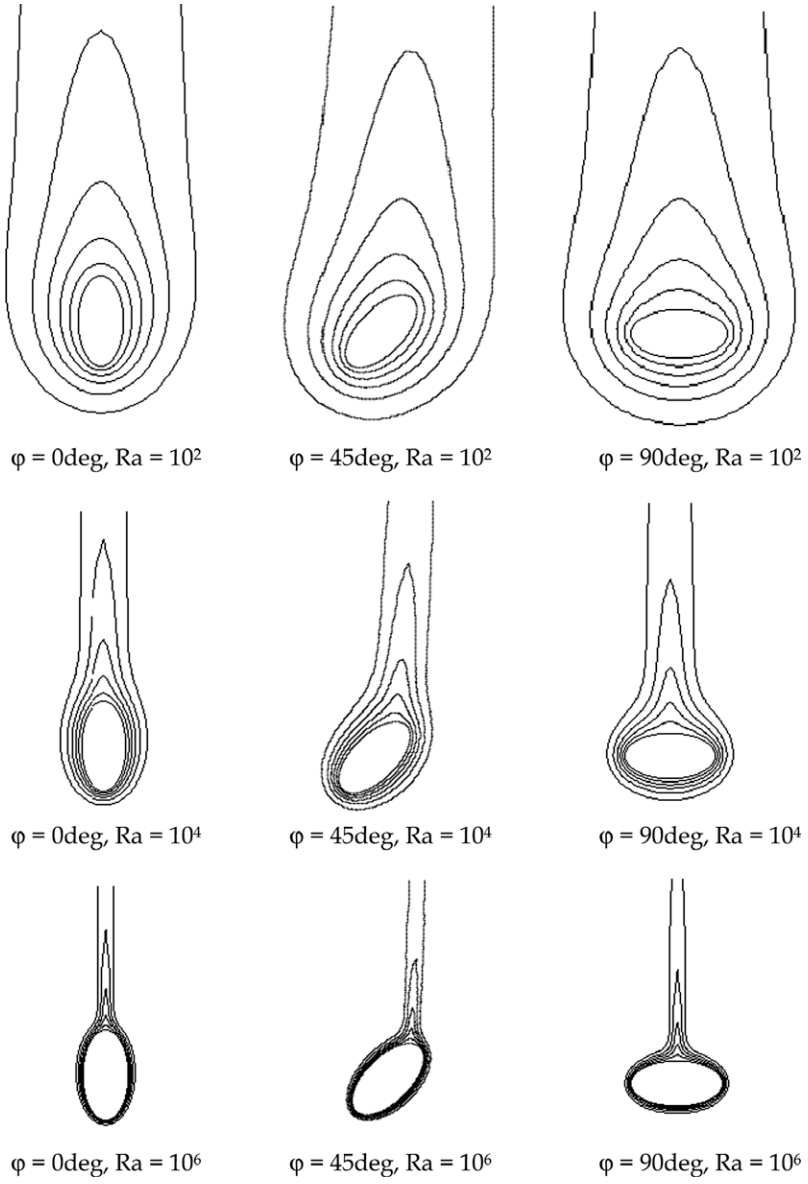

Fig. 12. Isotherm contour plots for $Pr = 0.7$, $b/a = 0.5$, $\varphi = 0$–90°, and $Ra = 10^2$to 10^6.

(a) for $\varphi < \varphi^* \cong 67.5^\circ$, $10 < Ra \leqslant 10^7$ and $0.7 \leqslant Pr \leqslant 700$

$$(b/a)_{\text{opt}} = \max[0.05, \psi_1(Ra, \varphi)] \tag{11}$$

where $\psi_1(Ra,\varphi)$ is given by:

$$\psi_1(Ra,\varphi) = 0.321\left\{[1 - 0.24Ra^{0.235}\sin(\varphi^* - \varphi)]^5 + 0.014 \times \exp(-0.0001Ra)\right\}^{0.2} \quad (\varphi \text{ and } \varphi^* \text{ in radians}) \tag{12}$$

with a 5.4% standard deviation of error and a ±9.6% range of error with a 90% level of confidence;

(b) for $\varphi \geqslant \varphi^* \cong 67.5^\circ$, $10 < Ra \leqslant 10^7$ and $0.7 \leqslant Pr \leqslant 700$

$$(b/a)_{\text{opt}} = \min[\psi_2(Ra, \varphi), 0.98] \tag{13}$$

where $\psi_2(Ra,\varphi)$ is given by:

$$\psi_2(Ra,\varphi) = 0.1 + 0.066\ln(Ra) \times [\sin(\varphi - \varphi^*)]^{0.187} \quad (\varphi \text{ and } \varphi^* \text{ in radians}) \tag{14}$$

with a 5.5% standard deviation of error and a ±8.2% range of error with a 90% level of confidence.

Note that in Eqs. (12) and (14) the orientation angles are expressed in radians.

4.4. Heat transfer correlations

The whole set of numerical results obtained for the average Nusselt number Nu may be correlated to the Rayleigh number, Ra, the axis ratio, b/a, the orientation angle of the elliptic cross-section, φ, and the Prandtl number, Pr, by the following binomial correlating equation, as shown in Fig. 21:

$$Nu = 0.66 + 0.535\{1 + f_1 + [(b/a) - 1]f_2\} \times \frac{Ra^{1/4}}{[1 + (0.49/Pr)^{9/16}]^{4/9}} \tag{15}$$

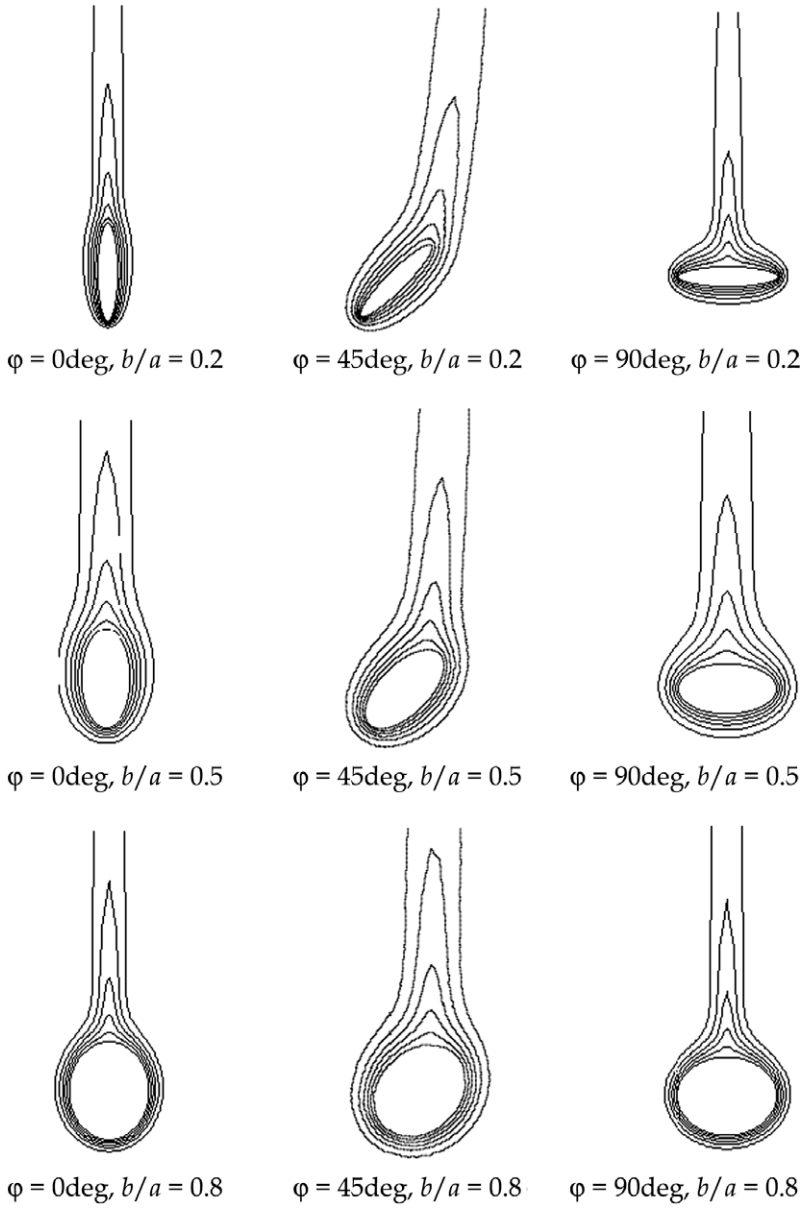

Fig. 13. Isotherm contour plots for $Pr = 0.7$, $Ra = 10^4$, $\varphi = 0$–90°, and $b/a = 0.2$–0.8.

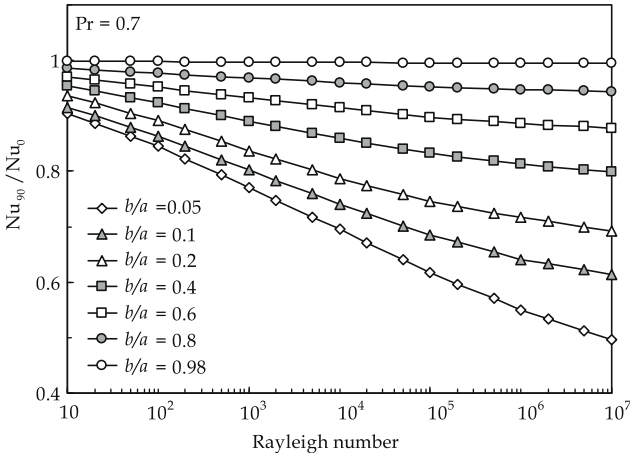

Fig. 14. Distributions of Nu_{90}/Nu_0 vs. Ra for $Pr = 0.7$ and different values of b/a.

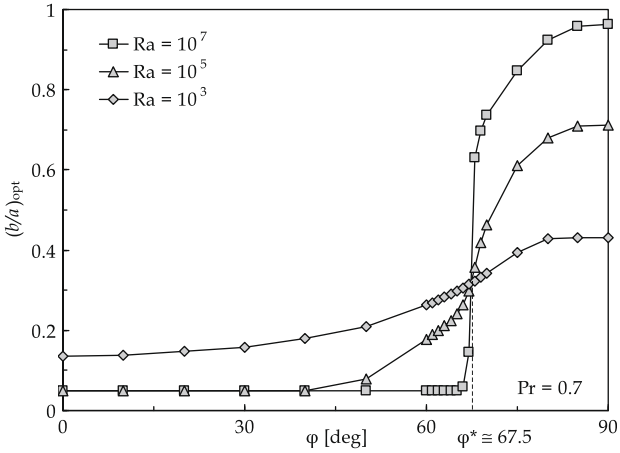

Fig. 15. Distributions of $(b/a)_{opt}$ vs. φ for $Pr = 0.7$ and different values of Ra.

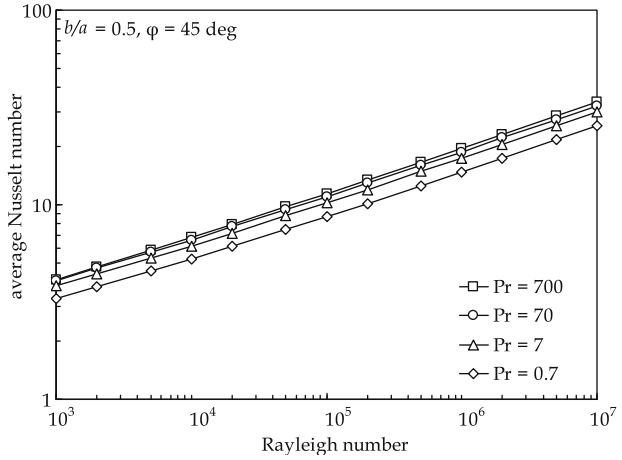

Fig. 16. Distributions of *Nu* vs. *Ra* for $b/a = 0.5$, $\varphi = 45°$ and different values of *Pr*.

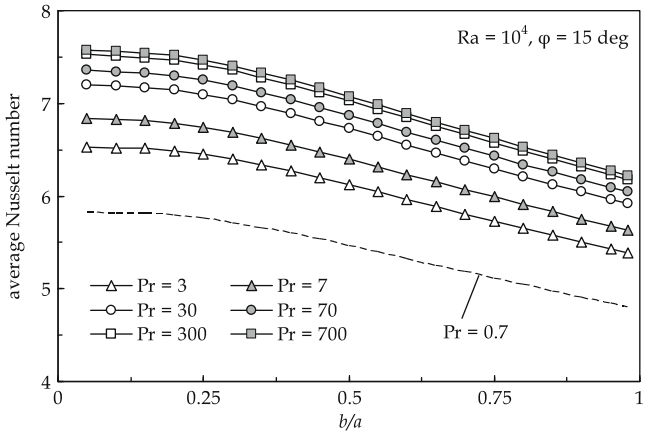

Fig. 17. Distributions of *Nu* vs. *b*/*a* for $Ra = 10^4$, $\varphi = 15°$ and different values of *Pr*.

for $10 \leqslant Ra \leqslant 10^7$, $0.05 \leqslant b/a \leqslant 0.98$, $0° \leqslant \varphi \leqslant 90°$, and $0.7 \leqslant Pr \leqslant 700$, where f_1 and f_2 are given by:

(a) for $\varphi < \varphi^* \cong 67.5°$ and $Ra \leqslant 10^4$

$$f_1 = -0.15\exp[-8.1(b/a)] \tag{16}$$

$$f_2 = 0.051(\sin\varphi)\log(Ra) - 0.43 \quad (\varphi \text{ in radians}) \tag{17}$$

with a 1.6% standard deviation of error and a ±3.4% range of error with a 95% level of confidence;

(b) for $\varphi < \varphi^* \cong 67.5°$ and $Ra > 10^4$

$$f_1 = -0.048\exp[-2.2(b/a)] \tag{18}$$

$$f_2 = 0.034(\sin\varphi)^2\log(Ra) - 0.31 \quad (\varphi \text{ in radians}) \tag{19}$$

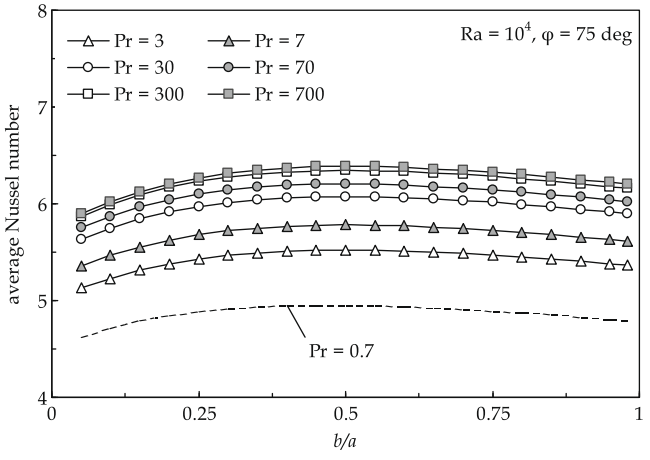

Fig. 18. Distributions of *Nu* vs. *b*/*a* for $Ra = 10^4$, $\varphi = 75°$ and different values of *Pr*.

with a 1.6% standard deviation of error and a ±2.9% range of error with a 95% level of confidence;

(c) for $\varphi \geqslant \varphi^* \cong 67.5°$ and $Ra \leqslant 10^4$

$$f_1 = 0.073\left\{Ra^{[\sin(\varphi-\varphi^*)]^{3.2}}\right\}\ln(b/a) \quad (\varphi \text{ and } \varphi^* \text{ in radians}) \tag{20}$$

$$f_2 = 0.044(\sin\varphi)^7\log(Ra) - 0.38 \quad (\varphi \text{ in radians}) \tag{21}$$

with a 1.9% standard deviation of error and a ±3.3% range of error with a 95% level of confidence;

(d) for $\varphi \geqslant \varphi^* \cong 67.5°$ and $Ra > 10^4$

$$f_1 = 0.063\left\{Ra^{[\sin(\varphi-\varphi^*)]^{3.3}}\right\}\ln(b/a) \quad (\varphi \text{ and } \varphi^* \text{ in radians}) \tag{22}$$

$$f_2 = 0.040(\sin\varphi)^7\log(Ra) - 0.30(\varphi \text{ in radians}) \tag{23}$$

with a 2.1% standard deviation of error and a ±3.9% range of error with a 95% level of confidence.

Note that in Eqs. (17) and (19)–(23) the orientation angles are expressed in radians.

5. Conclusions

Steady laminar free convection from horizontal elliptic cylinders set in unbounded space has been studied numerically through a specifically developed computer-code based on the SIMPLE-C algorithm, under the assumption of uniform surface temperature. Simulations have been performed for ratios between the minor and major axes of the elliptic cross-section of the cylinder in the

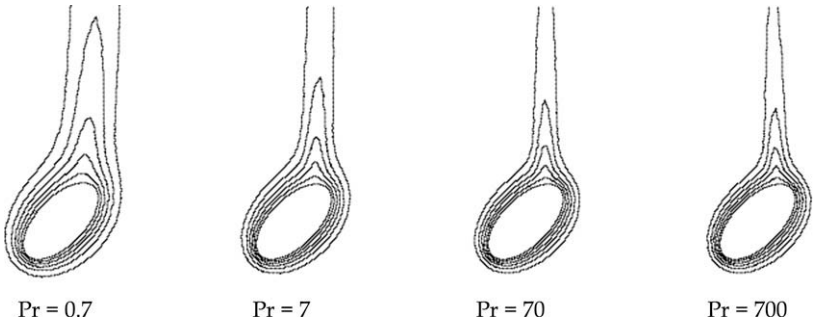

Fig. 19. Isotherm contour plots for $Ra = 10^4$, $b/a = 0.5$, $\varphi = 45°$, and $Pr = 0.7$–700.

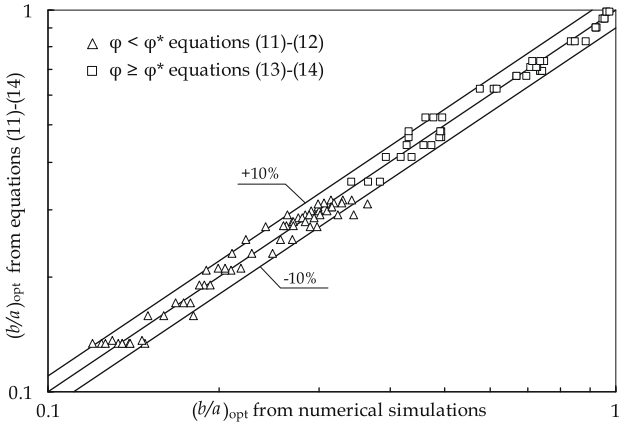

Fig. 20. Comparison between Eqs. (11)–(14) and the numerical results.

range between 0.05 and 0.98, inclination angles of the major axis of the elliptic cross-section with respect to gravity in the range between 0° and 90°, Rayleigh numbers based on the major axis of the elliptic cross-section in the range between 10 and 10^7, and Prandtl numbers in the range between 0.7 and 700. New dimensionless correlating equations with good standard deviations of error and sufficiently narrow ranges of error for quite acceptable levels of confidence, have been developed for the average Nusselt number and the optimum axis ratio for maximum heat transfer from the cylinder surface to the undisturbed surrounding fluid reservoir.

The main results obtained in the present study may be summarized as follows:

(a) The average Nusselt number increases with increasing the Rayleigh number, with a slope which decreases or increases with increasing the axis ratio, depending on whether the tube configuration is either slender or blunt.
(b) The average Nusselt number increases with increasing the Prandtl number, with a decreasing gradient.
(c) The average Nusselt number decreases with increasing the orientation angle of the elliptic cross-section of the cylinder, with a slope which increases as the Rayleigh number increases and the axis ratio decreases.
(d) In most cases, the average Nusselt number has a peak at an optimum axis ratio which increases or decreases with increasing the Rayleigh number, depending on whether the orientation angle of the tube is above or below a critical value of approximately 67.5°, independently of both the Rayleigh and Prandtl numbers, at which the optimum axis ratio is nearly 0.33, independently of both the Rayleigh and Prandtl numbers.

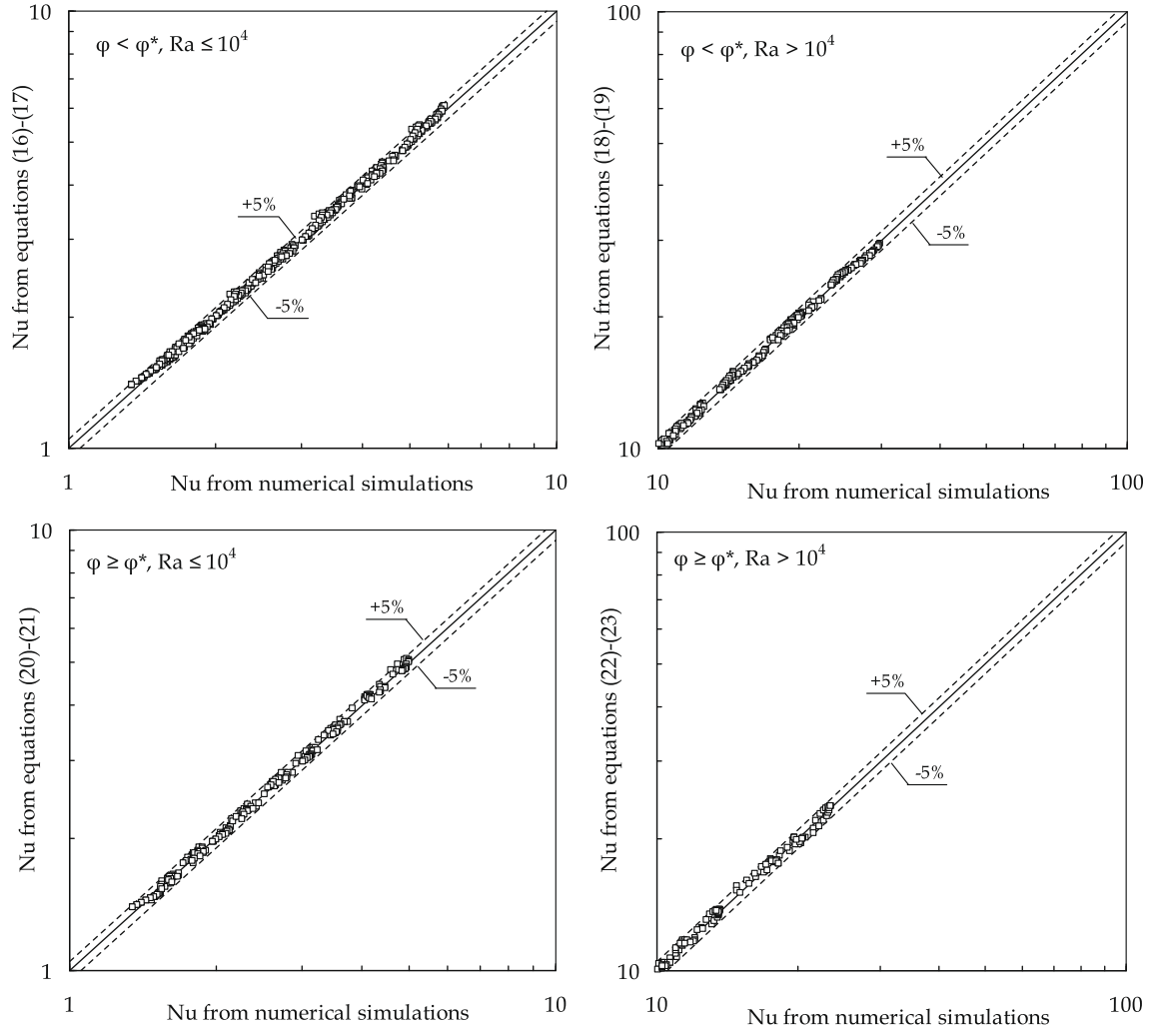

Fig. 21. Comparison between Eqs. (16)–(23) and the numerical results.

(e) At any Rayleigh number and orientation of the elliptic cross-section with respect to gravity, the optimum axis ratio for maximum heat transfer from the cylinder surface to the undisturbed fluid reservoir is practically independent of the Prandtl number.

References

[1] I. Langmuir, Convection and conduction in gases, Phys. Rev. XXXIV (1912) 401–422.
[2] W.H. McAdams, Heat Transmission, McGraw-Hill, New York, 1954.
[3] V.T. Morgan, The overall convective heat transfer from smooth circular cylinders, Adv. Heat Transfer 11 (1975) 199–264.
[4] S.W. Churchill, H.H.S. Chu, Correlating equations for laminar and turbulent free convection from a horizontal cylinder, Int. J. Heat Mass Transfer 18 (1975) 1049–1053.
[5] T.H. Kuehn, R.J. Goldstein, Correlating equations for natural convection heat transfer between horizontal circular cylinders, Int. J. Heat Mass Transfer 19 (1976) 1127–1134.
[6] S.S. Kutateladze, Fundamentals of Heat Transfer, Academic Press, New York, 1963.
[7] L. Pera, B. Gebhart, Experimental observations of wake formation over cylindrical surfaces in natural convection flows, Int. J. Heat Mass Transfer 15 (1972) 175–177.
[8] G. Hesse, E.M. Sparrow, Low Rayleigh number natural convection heat transfer from high-temperature horizontal wires to gases, Int. J. Heat Mass Transfer 17 (1974) 796–798.
[9] R.M. Fand, E.W. Morris, M. Lum, Natural convection heat transfer from horizontal cylinders to air water and silicone oils for Rayleigh numbers between 3×10^2 and 2×10^7, Int. J. Heat Mass Transfer 20 (1977) 1173–1184.
[10] S.B. Clemes, K.G.T. Hollands, A.P. Brunger, Natural convection heat transfer from long horizontal isothermal cylinders, J. Heat Transfer 116 (1994) 96–104.
[11] R. Hermann, Heat transfer by free convection from horizontal cylinders in diatomic gases, NACA TM 1366, 1954.
[12] T. Chiang, J. Kaye, On laminar free convection from a horizontal cylinder, in: Proceedings of the Fourth National Congress of Applied Mechanics, 1962, pp. 1213–1219.
[13] D.A. Saville, S.W. Churchill, Laminar free convection in boundary layers near horizontal cylinders and vertical axisymmetric bodies, J. Fluid Mech. 29 (1967) 391–399.
[14] L. Elliot, Free convection on a two-dimensional or axisymmetric body, Q. J. Mech. Appl. Math. 23 (1970) 153–162.
[15] J.H. Merkin, Free convection on an isothermal horizontal cylinder, ASME Paper No. 76-HT-16, 1976.
[16] M.A. Muntasser, J.C. Mulligan, A local non-similarity analysis of free convection from a horizontal cylindrical surface, J. Heat Transfer 100 (1978) 165–167.
[17] T.H. Kuehn, R.J. Goldstein, Numerical solution to the Navier–Stokes equations for laminar natural convection about a horizontal isothermal circular cylinder, Int. J. Heat Mass Transfer 23 (1980) 971–979.
[18] B. Farouk, S.I. Guceri, Natural convection from a horizontal cylinder-laminar regime, J. Heat Transfer 103 (1981) 522–527.
[19] H.M. Badr, Heat transfer in transient buoyancy driven flow adjacent to a horizontal rod, Int. J. Heat Mass Transfer 30 (1987) 1997–2012.
[20] P. Wang, R. Kahawita, T.H. Nguyen, Numerical computation of the natural convection flow about a horizontal cylinder using splines, Numer. Heat Transfer 17 (1990) 191–215.
[21] T. Saitoh, T. Sajiki, K. Maruhara, Bench mark solutions to natural convection heat transfer problem around a horizontal circular cylinder, Int. J. Heat Mass Transfer 36 (1993) 1251–1259.
[22] F.N. Lin, B.T. Chao, Laminar free convection over two-dimensional and axisymmetric bodies of arbitrary contour, J. Heat Transfer 96 (1974) 435–442.
[23] G.D. Raithby, K.G.T. Hollands, Laminar and turbulent free convection from elliptic cylinders with a vertical plate and horizontal circular cylinder as special cases, J. Heat Transfer 98 (1976) 72–80.
[24] A.V. Hassani, Natural convection heat transfer from cylinders of arbitrary cross section, J. Heat Transfer 114 (1992) 768–773.
[25] J.H. Merkin, Free convection boundary layers on cylinders of elliptic cross section, J. Heat Transfer 99 (1977) 453–457.
[26] C.-Y. Cheng, The effect of temperature-dependent viscosity on the natural convection heat transfer from a horizontal isothermal cylinder of elliptic cross section, Int. Commun. Heat Mass Transfer 33 (2006) 1021–1028.
[27] S.Y. Huang, F. Mayinger, Warmeubergang bei freier Konvektion um elliptische Rohre, Warme Stoffubertrag. 18 (1984) 175–183.
[28] H.M. Badr, K. Shamsher, Free convection from an elliptic cylinder with major axis vertical, Int. J. Heat Mass Transfer 36 (1993) 3593–3602.
[29] Y.-M. Chen, K.-C. Wang, Numerical and experimental studies on natural convection from a horizontal elliptic cylinder, J. Chin. Inst. Chem. Eng. 27 (1996) 353–362.
[30] H.M. Badr, Laminar natural convection from an elliptic tube with different orientations, J. Heat Transfer 119 (1997) 709–718.
[31] F.M. Mahfouz, S. Kocabiyik, Transient numerical simulation of buoyancy driven flow adjacent to an elliptic tube, Int. J. Heat Fluid Flow 24 (2003) 864–873.
[32] A.O. Elsayed, E.Z. Ibrahim, S.A. Elsayed, Free convection from a constant heat flux elliptic tube, Energy Convers. Manage. 44 (2003) 2445–2453.
[33] J.P. Van Doormaal, G.D. Raithby, Enhancements of the simple method for predicting incompressible fluid flows, Numer. Heat Transfer 11 (1984) 147–163.
[34] S.V. Patankar, D.B. Spalding, A calculation procedure for heat mass and momentum transfer in three-dimensional parabolic flows, Int. J. Heat Mass Transfer 15 (1972) 1787–1797.
[35] B.P. Leonard, A stable and accurate convective modelling procedure based on quadratic upstream interpolation, Comput. Meth. Appl. Mech. Eng. 19 (1979) 59–78.
[36] S.V. Patankar, Numerical Heat Transfer and Fluid Flow, Hemisphere, Washington, DC, 1980.
[37] S.V. Patankar, Recent developments in computational heat transfer, J. Heat Transfer 110 (1988) 1037–1045.
[38] S. Ramanujan, Modular equations and approximations to π, Quart. J. Pure Appl. Math. 45 (1913–1914) 350–372.
[39] C. Cianfrini, M. Corcione, E. Habib, Free convection heat transfer from a horizontal cylinder affected by a downstream parallel cylinder of different diameter, Int. J. Therm. Sci. 45 (2006) 923–931.